

# Self-Assembly of Model DNA-Binding Peptide Amphiphiles

Ronit Bitton,<sup>†</sup> Judith Schmidt,<sup>‡</sup> Markus Biesalski,<sup>§</sup> Raymond Tu,<sup>||</sup>  
Matthew Tirrell,<sup>||</sup> and Havazelet Bianco-Peled<sup>\*‡</sup>

*Inter-Departmental Program for Biotechnology and Department of Chemical Engineering, Technion-Israel Institute of Technology, Israel, Department of Chemistry and Physics of Interfaces, Institute for Microsystem Technology (IMTEK), University of Freiburg, Germany, and Departments of Chemical Engineering and Materials, University of California, Santa Barbara, California*

Received July 6, 2005. In Final Form: August 31, 2005

Peptide amphiphiles combine the specific functionality of proteins with the engineering convenience of synthetic amphiphiles. These molecules covalently link a peptide headgroup, typically from an active fragment of a larger protein, to a hydrophobic alkyl tail. Our research is aimed at forming and characterizing covalently stabilized, self-assembled, peptide-amphiphile aggregates that can be used as a platform for the examination and modular design and construction of systems with engineering biological activity. We have studied the self-assembly properties of a model DNA-binding amphiphile, having a GCN4 peptide as the headgroup and containing a polymerizable methacrylic group in the tail region, using a combination of small-angle X-ray scattering, small-angle neutron scattering, and cryo-transmission electron microscopy. Our results reveal a variety of morphologies in this system. The peptide amphiphiles assembled in aqueous solution to helical ribbons and tubules. These structures transformed into lamella upon DNA binding. In contrast with common surfactants, the specific interaction between the headgroups seems to play an important role in determining the microstructure. The geometry of the self-assembled aggregate can be controlled by means of adding a cosurfactant. For example, the addition of SDS induced the formation of spherical micelles.

## Introduction

Proper performance of biological systems depends on their ability to specifically assemble molecules in a complex environment that includes a variety of components and membrane-bound compartments. Peptide amphiphiles with targeted bioactivity were first designed and developed to mimic this machinery with a synthetic molecule that combines a peptide headgroup covalently linked to a hydrocarbon tail.<sup>1</sup> The amphiphilic architecture can be designed to contain various hydrophobic tail lengths and geometries attached to a biospecific peptide structure, allowing us to study dispersed phase aggregates and to control the assembled structures by manipulating their molecular construction in a modular fashion.

The first generation of peptide amphiphiles covalently linked a peptide headgroup, typically an active fragment of a larger protein with a propensity to form a distinct secondary structural element, to a hydrophobic saturated alkyl tail. The tails provide a hydrophobic moiety, promoting self-association and/or interaction with surfaces and interfaces.<sup>1–4</sup> This localization and alignment of peptide strands has been shown to promote the formation of protein-like secondary structure, such as  $\alpha$ -helices, or super-secondary structures such as coiled-coil  $\alpha$ -helices and triple helices, even in relatively short peptides that

do not order on their own.<sup>3–8</sup> Moreover, surfaces that were modified by attaching peptide amphiphiles were shown to provide functionality similar to that of the native protein from which the peptide sequence was taken.<sup>7–12</sup>

As with any surfactant, peptide amphiphiles self-assemble in aqueous solution and form a variety of complex structures. Exploring the shape of these aggregates piques basic scientific curiosity, for example, toward further understanding of the control of geometry of micellar structures. Moreover, previous studies have shown that the biological activity of the peptide headgroup can be affected by the aggregate geometry.<sup>10</sup> As early as the mid-eighties, Ihara et al.<sup>13</sup> have shown that peptide amphiphiles having L-aspartic acid headgroups are capable of forming globular structures that transform to twisted ribbonlike aggregates.<sup>13</sup> In the early nineties Shimizu and Hato<sup>14</sup> showed that molecules, such as HCl·H-Sar-Sar-Sar-Glu(NHC12)-NHC12, with a planar zigzag head-

\* To whom correspondence should be addressed. E-mail: bianco@tx.technion.ac.il.

<sup>†</sup> Inter-Departmental Program for Biotechnology, Technion-Israel Institute of Technology.

<sup>‡</sup> Department of Chemical Engineering, Technion-Israel Institute of Technology.

<sup>§</sup> Institute for Microsystems Technology, University of Freiburg.

<sup>||</sup> Departments of Chemical Engineering and Materials, University of California.

(1) Berndt, P.; Fields, G. B.; Tirrell, M. *J. Am. Chem. Soc.* **1995**, *117*, 9515.

(2) Yu, Y.-C.; Pakalns, T.; Dori, Y.; McCarthy, J. B.; Tirrell, M.; Fields, G. B. *Methods Enzymol.* **1997**, *289*, 571.

(3) Yu, Y.-C.; Tirrell, M.; Fields, G. B. *J. Am. Chem. Soc.* **1998**, *120*, 9979.

(4) Fields, G. B.; Lauer, J. L.; Dori, Y.; Forns, P.; Yu, Y.-C.; Tirrell, M. *Biopolymers* **1998**, *47*, 143.

(5) Forns, P.; Fields, G. B. *Polym. Prepr.* **2000**, *41*, 1152.

(6) Forns, P.; Lauer-Fields, J. L.; Gao, S.; Fields, G. B. *Biopolymers* **2000**, *54*, 531.

(7) Tu, R. S.; Tirrell, M. *Adv. Drug Delivery Rev.* **2004**, *56*, 1537.

(8) Pakalns, T.; Haverstick, K. L.; Fields, G. B.; McCarthy, J. B.; Mooradian, D. L.; Tirrell, M. *Biomaterials* **1999**, *20*, 2265.

(9) Haverstick, K.; Pakalns, T.; Yu, Y.-C.; McCarthy, J. B.; Fields, G. B.; Tirrell, M. *PMSE* **1997**, *77*, 584.

(10) Lee, K. C.; Carlson, P. A.; Goldstein, A. S.; Yager, P.; Gelb, M. H. *Langmuir* **1999**, *15*, 5500.

(11) Dori, Y.; Bianco-Peled, H.; Satija, S. K.; Fields, G. B.; McCarthy, J. B.; Tirrell, M. *J. Biomed. Mater. Res.* **2000**, *50*, 75.

(12) Bianco-Peled, H.; Dori, Y.; Schneider, J.; Sung, L.-P.; Satija, S.; Tirrell, M. *Langmuir* **2001**, *17*, 6931.

(13) Ihara, H.; Fukumoto, T.; Hirayama, C.; Yamada, K. *Polym. Commun.* **1986**, *27*, 282.

(14) Shimizu, T.; Hato, M. *Biochim. Biophys. Acta* **1993**, *1147*, 50.

group conformation formed twisted ribbonlike aggregates but similar molecules with left helical headgroup conformation led to the formation of tubules and helical ribbonlike aggregates (HCl·H-Pro-Pro-Glu(NHC12)-NHC12) or stable vesicles (HCl·H-Pro-Pro-Pro-Glu(NHC12)-NHC12). On the basis of these results, it was concluded that the chirality of the amino acid residue and the headgroup volume may be determinants in the geometry of the formed assembly.<sup>14</sup> Hartgernik et al.<sup>15</sup> exploited the typical self-assembly of peptide amphiphiles capable of recreating the structural orientation between collagen and hydroxyapatite observed in bone. Twelve variants of these peptide amphiphiles have been shown to assemble into stable cylindrical micelles, which further assembled into nanofiber networks, resulting in the formation of aqueous gels.<sup>15</sup> Cholesterol-containing peptide amphiphiles have also demonstrated their ability to form nanofibers.<sup>16</sup> Although both  $\alpha$ -helices and  $\beta$ -sheets existed in the peptide, secondary structure was not of primary importance to the biomimetic function in these cases.

An important question that remains to be answered is how the secondary structure of the peptide influences the aggregation behavior and vice versa.<sup>17</sup> The authors are aware of only one paper describing the self-assembly properties of peptide amphiphiles in which the peptide folds into a distinct super-secondary structure.<sup>18</sup> This study focused on model collagen peptide amphiphiles made by attaching monoalkyl and dialkyl tails to a triple-helical-forming headgroup. These studies show that monoalkyl tails (c12–c18) conjugated to triple-helical-peptide headgroups all lead to the self-assembly of spherical micelles, while dialkyl tails lead to the formation of spherical micelles (c12) and disklike micelles (c16 and c18). Additionally, these disklike micelles aggregate in a nearly linear fashion to form supramolecular stacks of disklike micelles.<sup>18</sup>

Recently, our group has investigated a DNA-binding peptide amphiphile that we term “bZip”.<sup>19</sup> These peptide amphiphiles include three components: the basic region of GCN4 (KDPAALKRAR NTEAARRSRA RKLQRMK-QLE),<sup>20</sup> a short coiled-coil nucleation sequence (AK-LAEIE)-K,<sup>4,21</sup> and a mono- or dialkyl tail. These molecules cooperatively bind to DNA giving an enhancement in  $\alpha$ -helical structure, where the hydrophobic moiety seems to promote the alignment of the peptide into a natively “standing” orientation. Preliminary small-angle neutron scattering experiments indicated that the bZip peptide amphiphile self-assembled into rodlike aggregates, whereas when the same peptide amphiphiles complex with DNA they formed lamellar aggregates.<sup>19</sup> This contribution focuses on the morphological behavior of peptide amphiphiles as micellar assemblies and complexed with DNA, where understanding the changes in phase associated with DNA binding to oligonucleotide sequences can be applied for DNA separations. We observe a distinct change in structure from cylindrical aggregates to larger length scale lamellar structures. However, for most practical applications, further stabilization of these assemblies may be

useful or essential. This can be achieved by the use of polymerizable hydrophobic tails,<sup>22</sup> furthering the analogy between peptide functional micelles and their protein analogues. In this work, we utilized small-angle X-ray scattering (SAXS), small-angle neutron scattering (SANS), and cryo-transmission electron microscopy (cryo-TEM) to investigate the self-assembly properties of polymerizable bZip peptide amphiphiles in water, DNA, and cosurfactant solutions.

## Materials and Methods

Sodium dodecyl sulfate, SDS (MW = 288.4 g/mol, purity 99%), was purchased from Sigma. Highly polymerized calf thymus DNA, obtained from Amersham Bioscience (Piscataway, NJ), was used for all DNA-binding experiments in 1x TAE buffer (40 mM Tris base, pH = 8.2). The molar concentrations shown below are based on the concentration of DNA base pairs [DNAbp], MW = 660 g/mol. Resin-bound bZip peptides were synthesized with Fmoc solid-phase methods by the Microchemical Facility at the University of Minnesota (Minneapolis, MN).

**Peptide-Amphiphile Synthesis.** Peptide amphiphiles were synthesized from resin-bound peptides with manual Fmoc solid-phase chemistry as described previously.<sup>1</sup> Peptide amphiphiles were purified by HPLC on reverse-phase C4 or C18 columns with gradients of acetonitrile in water with 0.1% TFA. The identity of purified peptide-amphiphile products was verified by MALDI-TOF mass spectrometry (peak position, MW = 4433 and 4701 for the bZip peptide and peptide amphiphile, respectively). Monoalkyl-methacrylic acid tails were synthesized by attaching a methacryloyl chloride to hydroxydodecanoic acid via an ester bond and, subsequently, forming amide bonds at the acid terminus of the tail. C-terminal lipidation was accomplished by protecting the  $\epsilon$ -amine group with a 1-(4,4-dimethyl-2,6-dioxocyclohexylidene)3-methylbutyl, Dde, and selectively deprotecting with 2% hydrazine monohydrate solution in DMF.<sup>23</sup> Dialkyl lipid-like tails were synthesized according to a protocol described by Berndt and co-workers.<sup>1</sup>

**Circular Dichroism (CD).** Prior to CD measurements, peptide concentration was verified by amino acid analysis at the Molecular Structure Facility (University of California-Davis) with Beckman 6300 amino acid analyzers. The secondary structure of the peptide was characterized with CD spectra on an Olis RSM 100 spectrophotometer (Bogart, GA) at 25 °C with 0.01, 0.05, and 0.1 cm path length quartz cuvettes, depending on the concentration of the peptide. A TAE buffer baseline was subtracted from each spectrum. Also, difference spectra were generated adjusting for DNA titrated into peptide mixtures by linearly subtracting the DNA spectrum proportional to the increase in concentration of DNA during titration.<sup>24,25</sup> Reported spectra are averages of four scans and are expressed as mean residue ellipticity,  $[\theta]$ . CD basis spectra were measured with poly(Lysine) and poly(Glutamic acid) (Sigma) with conditions and parameters reported by others.<sup>26,27</sup> Linear combinations of  $\alpha$ -helix,  $\beta$ -sheet, and random coil basis spectra are used to fit experimental CD spectra for the estimation of secondary structure contributions. CD measurements for peptide amphiphiles and peptide alone are taken at 0.1 mM. The peptide amphiphiles were subsequently complexed with high-molecular-weight calf-thymus DNA (ctDNA) at 50  $\mu$ M base pairs (660 g/mol for each base-pair) in a 1x TAE buffer (40 mM Tris at pH = 8.2). As DNA was added to 0.1 mM m16-bZip and d16-bZip, the solution became bluish and more opaque, attenuating the intensity of absorbed light; therefore, soluble peptide concentrations are monitored

(15) Hartgerink, J. D.; Beniash, E.; Stupp, S. I. *PNAS* **2002**, *99*, 5133.

(16) Guler, M. O.; Rabatic, B. M.; Claussen, R. C.; Stupp, S. I. *Polym. Prepr.* **2003**, *44*, 102.

(17) Loewik, D. W. P. M.; van Hest, J. C. M. *Chem. Soc. Rev.* **2004**, *33*, 234.

(18) Gore, T.; Dori, Y.; Talmon, Y.; Tirrell, M.; Bianco-Peled, H. *Langmuir* **2001**, *17*, 5352.

(19) Tu, R. S. In preparation, 2005.

(20) Ellenberger, T. E.; Brandl, C. J.; Struhl, K.; Harrison, S. C. *Cell* **1992**, *71*, 1223.

(21) Su, J. Y.; Hodges, R. S.; Kay, C. M. *Biochemistry* **1994**, *33*, 15501.

(22) Biesalski, M.; Tu, R.; Tirrell, M. V. *Langmuir* **2005**, *21*, 5663.

(23) Chhabra, S. R.; Hothi, B.; Evans, D. J.; White, P. D.; Bycroft, B. W.; Chan, W. C. *Tetrahedron Lett.* **1998**, *39*, 1603.

(24) Cuenoud, B.; Schepartz, A. *Science* **1993**, *259*, 510.

(25) Weiss, M. A.; Ellenberger, T.; Wobbe, C. R.; Lee, J. P.; Harrison, S. C.; Struhl, K. *Nature* **1990**, *347*, 575.

(26) Greenfield, N. J.; Fasman, G. D. *Biochemistry* **1969**, *8*, 4108.

(27) Adler, A. J.; Greenfield, N. J.; Fasman, G. D. *Methods Enzymol.* **1973**, *27*, 675.



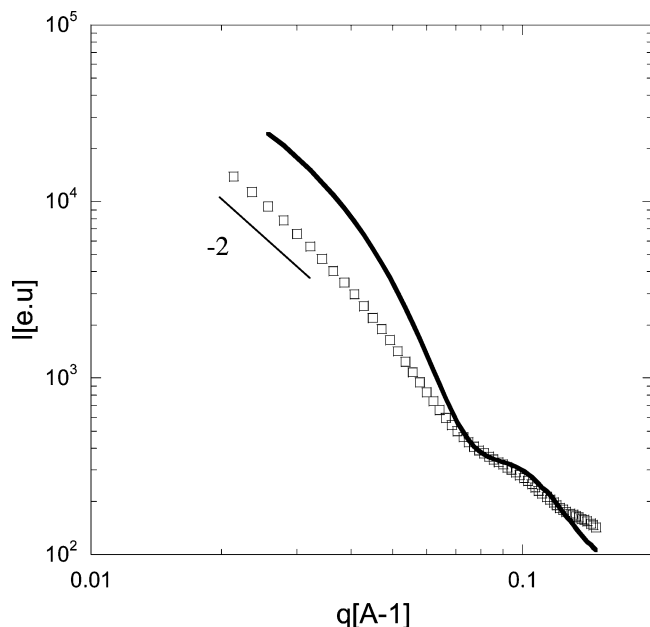


**Figure 4.** Desmeared SAXS curve of 3.3 mM MMA-bZip in aqueous solution ( $\diamond$  experimental points) fitted to a core-shell, polydisperse, cylindrical micelle model (— solid curve).

## Results and Discussion

### Self-Assembly of MMA-bZip in Aqueous Solution.

MMA-bZip, the bZip peptide amphiphile designed for this study, is shown in Figure 1.

The secondary structure of these amphiphiles in solution is evaluated with CD spectroscopy (Figure 2) and is similar to other bZip peptide amphiphiles.<sup>19</sup> The  $\alpha$ -helicity of MMA-bZip peptide amphiphiles above the critical micelle concentrations is 57%, which is significantly higher when compared to the unalkylated bZip peptide alone, containing an  $\alpha$ -helicity of only 33%.

Single-tail surfactants often form spherical micelles. However, in a cryo-TEM micrograph of a 3.3 mM MMA-bZip vitrified solution (Figure 3), one can see a coexistence of elongated objects and a smaller number of helical ribbons. The spherical micelles that were expected are not observed.

Initially, one may hypothesize that the elongated objects seen in the cryo-TEM micrograph are cylindrical micelles. The scattering intensity from a solution containing concentric core-shell cylindrical structures, whose inner radius is normally distributed, can be calculated using the appropriate form factor in eq 3, which then takes the form

$$I(q) = N \int_0^\infty \frac{\pi L}{q} \left[ \Delta\rho_S R_S^2 \pi \frac{2J_1(qR_S)}{(qR_S)} + (\Delta\rho_C - \Delta\rho_S) R_C^2 \pi \frac{2J_1(qR_C)}{(qR_C)} \right]^2 (2\pi\sigma^2)^{-1/2} \exp[-(R_C - \bar{R}_C)^2/2\sigma^2] d(R_C) \quad (4)$$

where  $J_1$  is a Bessel function of a first order,  $R_S$  and  $R_C$  are the outer and inner (core) radii,  $\rho_S$  and  $\rho_C$  are the electron densities of the shell and the core, respectively,  $\rho_m$  is the electron density of the medium,  $\Delta\rho_S = \rho_S - \rho_m$ , and  $\Delta\rho_C = \rho_C - \rho_m$ .

The best fit of this model to the experimental SAXS data is shown as a solid line in Figure 4. Clearly, the model of cylindrical micelles fails to give a reasonable fit to the experimental data. Yet, a  $q^{-1}$  dependence for rods exists at higher  $q$  values, while at low  $q$  values, the scattering curve exhibits a  $q^{-2}$  behavior which may indicate lamellar structures. Taken together, these observations lead us to believe that the actual microstructure is a combination of a lamellar structure and a cylinder, such as a tubule. In pure geometrical terms, a tubule is a hollow, layered cylindrical object with three different electron densities along the radius, as shown schematically in Figure 5:

The scattering from a tubule can be calculated from a modification of eq 4 that takes into account all four layers. The scattering intensity of a single tubule is represented in eq 5

$$i_0(q, R_S, R_C) = \frac{\pi^3 L}{q} I_1^2(q)$$

$$I_1(q) = \Delta\rho_1 R_1^2 \frac{2J_1(qR_1)}{(qR_1)} + \Delta\rho_2 R_2^2 \frac{2J_1(qR_2)}{(qR_2)} - \Delta\rho_2 R_1^2 \frac{2J_1(qR_1)}{(qR_1)} + \Delta\rho_3 R_3^2 \frac{2J_1(qR_3)}{(qR_3)} - \Delta\rho_3 R_2^2 \frac{2J_1(qR_2)}{(qR_2)} + \Delta\rho_2 R_4^2 \frac{2J_1(qR_4)}{(qR_4)} - \Delta\rho_2 R_3^2 \frac{2J_1(qR_3)}{(qR_3)} \quad (5)$$

The fitting of this model to the experimental SAXS data was performed using a minimum least-squares error procedure keeping a constant value of  $\rho_w = 333.3 \text{ e/nm}^3$  for the electron density of water.<sup>31</sup> The inner radius was assumed to be normally distributed. The best fit to eq 5, shown as a dashed line in Figure 6, was calculated using the parameters summarized in Table 1. We note that only positive  $R_1$  values were allowed. An average radius of 0 nm indicates that normal distribution might not be the best distribution function for the inner radii. Several other

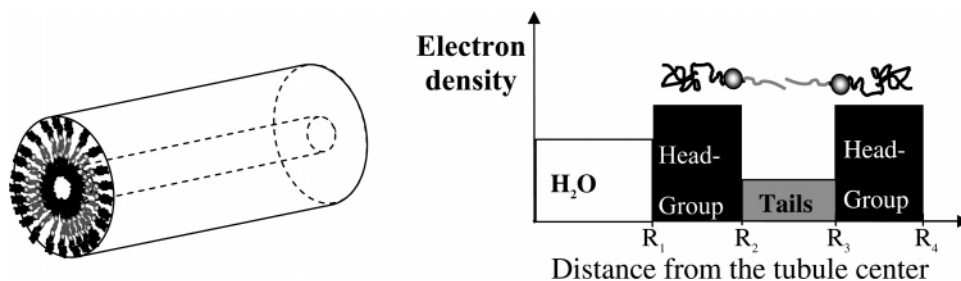


**Figure 5.** Electron density profile of a tubule (hollow cylinder).

**Table 1. Model Fit Parameters for MMA–bZip Solutions**

	SAXS	SANS	
	3.3 mM in H <sub>2</sub> O	0.5 mM in D <sub>2</sub> O	0.5 mM in 65:35 D <sub>2</sub> O/H <sub>2</sub> O mixture
electron/scattering length density of headgroup region, $\rho_1$	343 e/nm <sup>3</sup>	$6.96 \times 10^{-6} \text{ \AA}^{-2}$	$6.96 \times 10^{-6} \text{ \AA}^{-2}$
electron/scattering length density of tail region, $\rho_2$	283 e/nm <sup>3</sup>	$-1.00 \times 10^{-7} \text{ \AA}^{-2}$	$-1.00 \times 10^{-7} \text{ \AA}^{-2}$
electron/scattering length density of the solvent, $\rho_s$	333 e/nm <sup>3</sup>	$6.36 \times 10^{-6} \text{ \AA}^{-2}$	$3.94 \times 10^{-6} \text{ \AA}^{-2}$
inner radius $R_1$	$0 \pm 1 \text{ \AA}$	$2.89 \times 10^{-15} \pm 2 \text{ \AA}$	$2.89 \times 10^{-15} \pm 2 \text{ \AA}$
standard deviation $\sigma$	$17 \pm 1 \text{ \AA}$	$9.6 \pm 1.5 \text{ \AA}$	$9.6 \pm 1.5 \text{ \AA}$
effective length of the headgroup, $t_1$	$6.5 \pm 1 \text{ \AA}$	$6 \pm 1 \text{ \AA}$	$6 \pm 1 \text{ \AA}$
effective length of tails $t_2$	$22 \pm 1 \text{ \AA}$	$22 \pm 1 \text{ \AA}$	$22 \pm 1 \text{ \AA}$
$\varphi \cdot l^a$	$7.66 \times 10^{-6}$	$1.3 \times 10^{-7}$	$1.3 \times 10^{-7}$

<sup>a</sup>  $\varphi$  is the number of tubules per unit volume and  $l$  is their length.

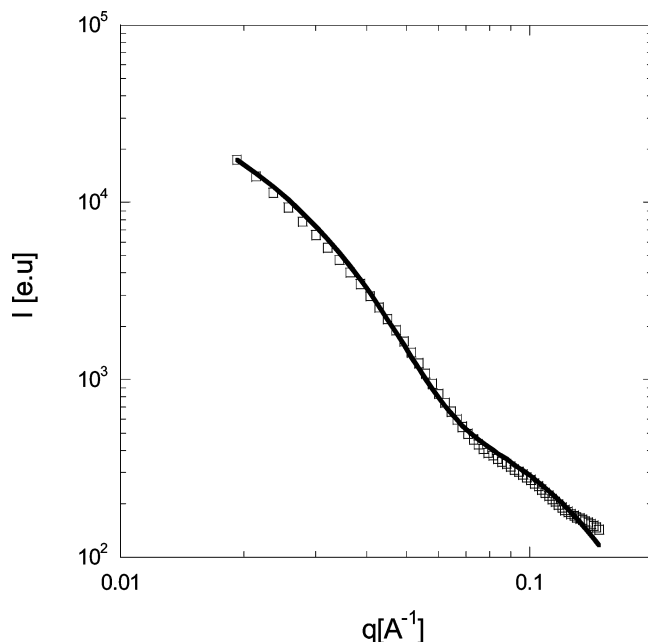


**Figure 6.** Desmeared SAXS curve of 3.3 mM MMA–bZip in aqueous solution ( $\diamond$  dotted curve) fitted to a polydispersed tubules model (– solid curve).

distribution functions (i.e., exponential distribution function) were examined (data not shown), however these functions gave not only the same quality of fit as the normal distribution function but similar obtained values as well. It should be emphasized, thus, that the size distribution is wide and most of the tubules have an inner radius that is much larger than zero. As evidence from the good fit of this model, it was justified to neglect the influence of the few helical ribbons seen in Figure 3 on the scattering pattern.

In addition to the consistency of the fitted parameters with the cryo-TEM images, further support of this model is gained by SANS measurements of 0.5 mM MMA–bZip in two solvents, pure D<sub>2</sub>O and a 65:35 D<sub>2</sub>O/H<sub>2</sub>O mixture. The tubule model is used to accurately fit the experimental data (Figure 7) yielding fit parameter values similar to those obtained with the SAXS parameters (Table 1).

Tubules are bilayer or multilayer membranes of amphiphilic molecules wrapped in a cylinder. Helical ribbons have similar microstructures, consisting of long twisted stripes of membranes with their edges exposed to the solvent.<sup>32</sup> In some cases, helical ribbons are unstable

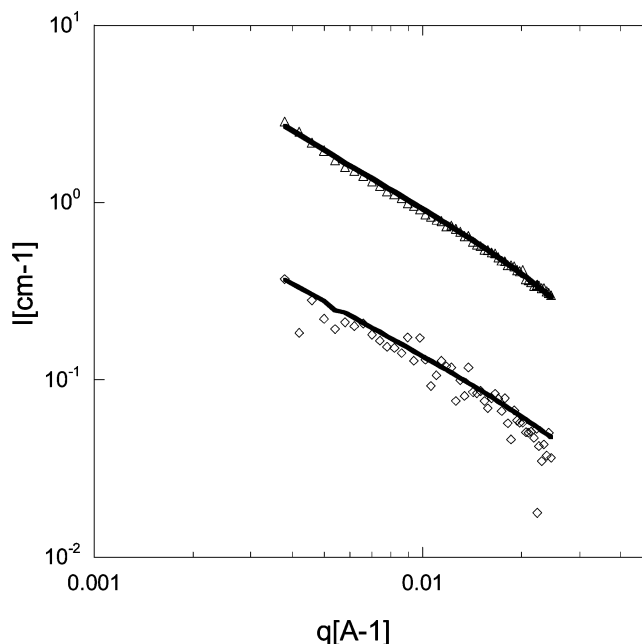


**Figure 7.** SANS curve of 0.5 mM MMA–bZip in D<sub>2</sub>O/H<sub>2</sub>O mixture ( $\diamond$ ) and D<sub>2</sub>O alone ( $\triangle$ ) fitted to a polydispersed tubules model (– solid curve).

precursors to the formation of tubules; in other cases, helical ribbons appear to be stable.<sup>32</sup> Tubule formation was also identified in surfactant-like peptides.<sup>33–35</sup> The theories describing tubules and helical ribbons formation which were recently reviewed by Selinger and co-workers<sup>36</sup> can be classified into two basic models: the first, the formation from chiral elastic properties of the membrane and the second, the formation from a variety of effects such as electrostatic interactions, elasticity of orientation order, and spontaneous curvature. From a comparison of theoretical calculations and relevant experimental work, it was found that the models based on chirality are more consistent with experimental results.<sup>36</sup> Since the MMA–bZip has a chiral, large headgroup, our results are consistent with the suggestion made in previous studies,<sup>14,18</sup> in which the chirality of the amino acid residue and the headgroup volume may be determinants in the geometry of the formed assemblies.

(33) von Maltzahn, G.; Vauthey, S.; Santoso, S.; Zhang, S. *Langmuir* **2003**, *19*, 4332.

(34) Santoso, S.; Hwang, W.; Hartman, H.; Zhang, S. *Nano Lett.* **2002**, *2*, 687.

(35) Vauthey, S.; Santoso, S.; Gong, H.; Watson, N.; Zhang, S. *PNAS* **2002**, *99*, 5355.

(36) Selinger, J. V.; Spector, M. S.; Schnur, J. M. *J. Phys. Chem. B* **2001**, *105*, 7157.

(32) Selinger, J. V.; MacKintosh, F. C.; Schnur, J. M. *Phys. Rev. E* **1996**, *53*, 3804.

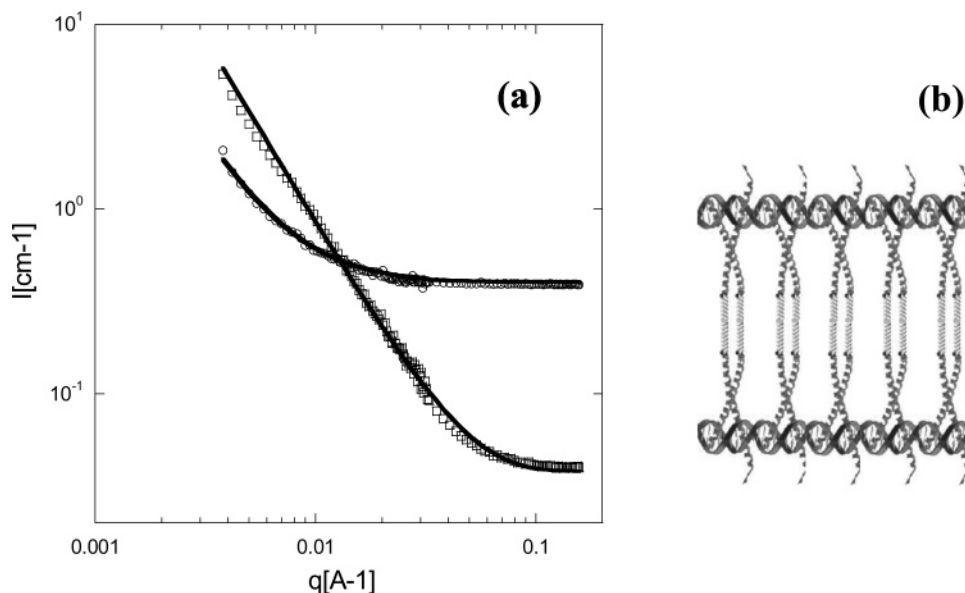


**Figure 8.** (a) SANS curve of the MMA-bZip/ctDNA complex in D<sub>2</sub>O/H<sub>2</sub>O mixture (○) and D<sub>2</sub>O alone (□) fitted to the lamellar core-shell model (— solid curve). (b) A schematic description of the lamellar structure.

**Table 2. Model Fit Parameters for MMA-bZip/CtDNA Complex Solutions**

	D <sub>2</sub> O	D <sub>2</sub> O/H <sub>2</sub> O
scattering length density of the core, $\rho_c$	$-1.00 \times 10^{-7} \text{ \AA}^{-2}$	$-1.00 \times 10^{-7} \text{ \AA}^{-2}$
scattering length density of the core, $\rho_s$	$5.03 \times 10^{-6} \text{ \AA}^{-2}$	$3.62 \times 10^{-6} \text{ \AA}^{-2}$
core thickness, $T_c$	$20 \pm 1 \text{ \AA}$	$20 \pm 1 \text{ \AA}$
shell thickness, $T_s$	$70 \pm 5 \text{ \AA}$	$70 \pm 5 \text{ \AA}$

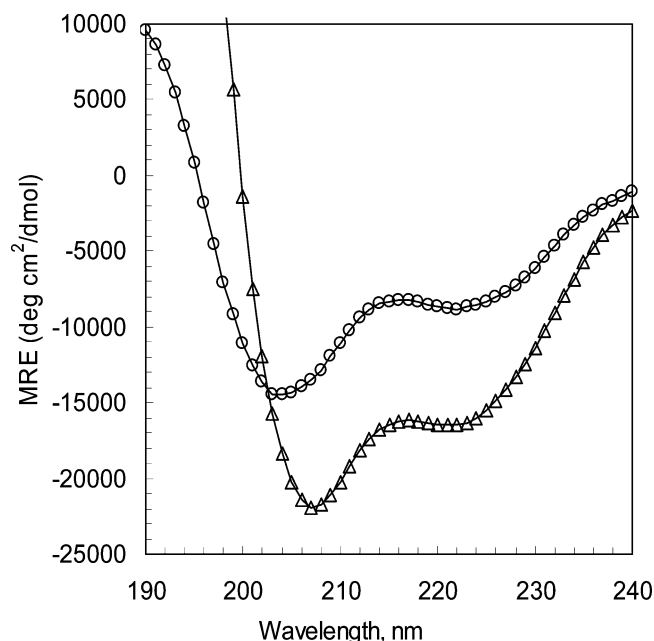


**Figure 9.** CD spectra of the bZip peptide only (○) and the MMA-bZip/SDS mixture (△).

**Self-Assembly of MMA-bZip/ctDNA Mixture in Aqueous Solution.** It was previously shown that mono- and dialkyl bZip peptide amphiphiles assemblies cooperatively bind to DNA.<sup>19</sup> These assemblies also rearrange upon DNA binding, possibly because of the strong electrostatic nature of the peptide-DNA interface, and we observe that MMA-bZip peptide amphiphiles show a similar behavior. SANS experiments (Figure 8) reveal that the addition of ctDNA results in significant changes in

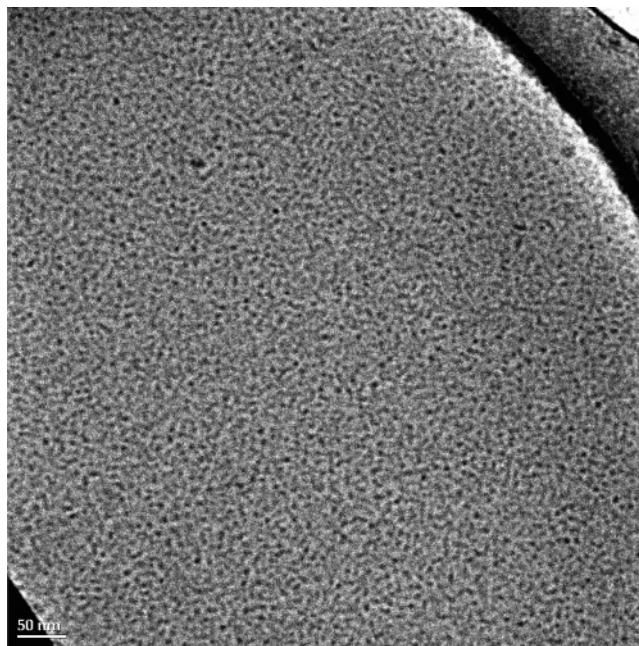


**Figure 10.** Cryo-TEM micrograph of 1.85 mM MMA-bZip and 83.3 mM SDS in aqueous solution.

the aggregate geometry. As a first guess, we assumed the bound DNA could be modeled as an additional layer of the tubule. However, this model could not be fitted to the data. Since the  $q^{-2}$  behavior at the low  $q$  range is still observed upon DNA binding, the scattering curves were fitted to a model of a membrane-like core-shell lamellar structure (see Figure 8) described by<sup>37</sup>

$$I(q) = A \frac{2\pi}{q^2} \left[ \Delta\rho_s T_s \frac{\sin(qT_s/2)}{qT_s/2} + (\Delta\rho_c - \Delta\rho_s) T_c \frac{\sin(qT_c/2)}{qT_c/2} \right]^2 \quad (6)$$

where  $T_s$  is the effective length of the headgroup and  $T_c$

(37) Pedersen, J. S. *Neutron, X-Ray Light Scattering* 2002, 391.

**Table 3. Model Fit Parameters for MMA–bZip/SDS Solutions**

	SDS/MMA–bZip	SDS
electron density of the shell, $\rho_s$	$445 \pm 2 \text{ e/nm}^3$	$448 \text{ e/nm}^3$
electron density of the core, $\rho_c$	$284 \pm 1 \text{ e/nm}^3$	$283 \text{ e/nm}^3$
volume fraction of the micelles, $\varphi$	$0.0011 \text{ nm}^3/\text{nm}^3$	$0.00092 \text{ nm}^3/\text{nm}^3$
core radius, $R_C$	$1.7 \pm 0.02 \text{ nm}$	$1.93 \text{ nm}$
shell thickness, $t$	$0.42 \pm 0.01 \text{ nm}$	$0.38 \pm 0.01 \text{ nm}$
standard deviation	$0.27 \pm 0.02 \text{ nm}$	

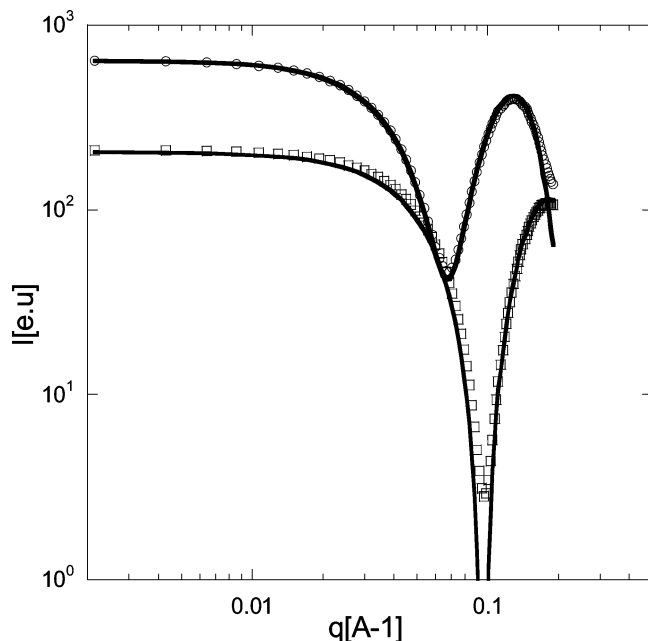


**Figure 11.** Desmeared SAXS curves of 1.85 mM MMA–bZip in aqueous solution ( $\diamond$ ) fitted to a core–shell, polydispersed, spherical micelle model (– solid curve) and 83.3 mM SDS in aqueous solution ( $\square$ ) fitted to a core–shell, monodispersed, spherical micelle model (– solid curve).

is the hydrophobic core thickness, representing two tails of a bilayer.

The best fit to eq 6 is shown as the solid line in Figure 8. This fit is obtained with the best-fit parameters given in Table 2, using constants scattering length densities of the solvent and the hydrophobic core. The scattering length density of the shell was assumed to be an average of the headgroup and the solvent densities with a hydration percentage of approximately 58%.

As previously mentioned, tubules are membranes of amphiphilic molecules wrapped in a cylinder. The binding of the DNA to the peptide headgroup promotes increased specific peptide–peptide interactions or generates a steric hindrance due to the alignment of the peptides along the polyelectrolyte that prevents the folding of the membrane into tubules. These results fortify the assumption that self-assembly is governed by the peptide headgroup.

**Self-Assembly of MMA–bZip/Cosurfactant Mixture in Aqueous Solution.** Self-assembly of peptide amphiphiles leads to the formation of aggregates having a high density of ligand on their surface. However, such a high density might not necessarily be optimal for all practical applications. For example, cell adhesion assays on monolayers of collagen-like peptide amphiphiles showed that molecular packing plays an important role in mediating cellular response.<sup>11</sup> To be able to serve as a template for cell adhesion, the peptide amphiphiles needed to be placed in a matrix of diluting, inert lipids.<sup>2</sup> Moreover, controlling the height differences between the peptide amphiphile and the nonfunctional lipid proved to be a beneficial way to manipulate the peptide accessibility of

the ligand to the cell receptors.<sup>11</sup> In self-assembled peptide amphiphile systems, forming mixed aggregates that contain both a peptide amphiphile and a cosurfactant could be exploited to control the density of the ligands on the aggregate surface. Furthermore, cosurfactants may be also used as a means to control the geometry of the self-assembled aggregate. With this in mind, we have added MMA–bZip to a solution that already consists of well-defined aggregates, hoping that the peptide amphiphile will insert itself into the existing aggregates without changing their shape. We chose SDS, an ionic surfactant known for forming spherical micelles, since it is a small molecule that will present an electrostatic repulsive surface to the DNA due to its negative charge.

Figure 9 shows the  $\alpha$ -helicity of MMA–bZip in the presence of SDS as a cosurfactant is higher than that of the bZip peptide alone (77% compared to 33%). In the TEM micrograph of 1.85 mM of MMA–bZip and 83.3 mM SDS solution, shown in Figure 10, there is no evidence of any aggregates other than small spherical micelles.

The experimental scattering curve was fitted to a model of spherical micelles whose inner radius is normally distributed

$$I(q) = \varphi \int_0^\infty \left[ \frac{4\pi}{3} \{ \Delta\rho_s R_s^3 \Phi(qR_s) + \Delta\rho_c R_c^3 \Phi(qR_c) - \Delta\rho_s R_c^3 \Phi(qR_c) \} \right]^2 (2\pi\sigma^2)^{-1/2} \exp[-(R_c - \bar{R}_c)^2/2\sigma^2] d(R_c) \quad (7)$$

where  $\Phi(h, R_i)$  is the single particle form factor for a sphere of radius  $R_i$

$$\Phi(q, R_i) = 3 \frac{\sin(qR_i) - hR_i \cos(qR_i)}{(qR_i)^3} \quad (8)$$

Figure 11 shows the experimental SAXS data. The solid line in this figure represents the calculated curve, obtained from eqs 7 and 8 using the best-fit parameters tabulated in Table 3. To ensure that the micelles are not pure SDS, we compared these values with the ones obtained from the scattering curve of the 83.3 mM SDS solution. The experimental data was well-fitted with a model of monodispersed core–shell spherical micelle, using values of  $\rho_w = 333.3 \text{ e/nm}^3$ ,  $\rho_c = 283 \text{ e/nm}^3$ , and  $\rho_s = 448$ <sup>38</sup> as the fixed parameters. The size of the micelles, tabulated in Table 3, are consistent with previously reported values.<sup>39</sup> The similarity between the size of the SDS micelles and the MMA–bZip/SDS mixed micelle, as well as the lack of larger aggregates in the TEM micrograph, indicate that only one or two molecules of MMA–bZip insert into each one of the SDS micelles.

## Conclusions

MMA–bZip peptide amphiphiles form tubules in aqueous solution, a phenomenon that seems to be driven at

(38) Suess, D.; Cohen, Y.; Talmon, Y. *Polymer* **1995**, *36*, 1809.

(39) Zemb, T.; Charpin, P. *J. Physiol. (Paris)* **1985**, *46*, 249.

least partly by interactions between the headgroups. Transformation of these aggregates into flat particles upon DNA binding seems to support the assumption that self-assembly properties are strongly influenced by the interactions between the headgroups, as the addition of DNA induces further folding to a fully helical conformation in the headgroup. MMA-bZip peptide amphiphiles could also be inserted into SDS micelles which remain spherical but do induce helical secondary structure in the peptide headgroup.

**Acknowledgment.** This work was partly supported by the United States–Israel Binational Science Foundation (Project 9900225 to H.B.-P. and M.T.). M.B. would like to thank the DFG (Deutsche Forschungsgemeinschaft) for a fellowship within the Emmy Noether Program, under Grant Number BI738/1-1. This work was supported in part at UC Santa Barbara by the NIRT and MRSEC Program of the National Science Foundation under Awards CTS-0103516 and DMR-0080034.

LA051811P